Journal of Solid Mechanics Vol. 3, No. 2 (2011) pp. 142-157

Time-Dependent Thermo-Electro-Mechanical Creep Behavior of Radially Polarized FGPM Rotating Cylinder

A. Ghorbanpour Arani[1,2,*], R. Kolahchi[1], A.A. Mosallaie Barzoki[1], A. Loghman[1]

[1]*Department of Mechanical Engineering, Faculty of Engineering, University of Kashan, Kashan, Iran*
[2]*Thermoelasticity Center of Excellence, Department of Mechanical Engineering, Amirkabir University of Technology, Tehran, Iran*

Received 1 May 2011; accepted 22 June 2011

ABSTRACT

Time-dependent creep analysis is crucial for the performance and reliability of piezoactuators used for high-precision positioning and load-bearing applications. In this study history of stresses, deformations and electric potential of hollow rotating cylinders made of functionally graded piezoelectric material (FGPM), e.g., PZT_7A have been investigated using Mendelson's method of successive elastic solution. Loading is composed of an internal pressure, a distributed temperature field, an inertia body force and a constant electric potential difference between the inner and outer surfaces of the FGPM cylinder. All the mechanical, thermal and piezoelectric properties are assumed to be the same power functions of the radial graded direction. Using equations of equilibrium, strain displacement, stress-strain relation and the electric potential equation a differential equation containing creep strains for displacement is derived. A semi-analytical method in conjunction with the method of successive approximation has therefore been proposed for this analysis. It has been found that a major redistribution for electric potential take place throughout the thickness. Electric potentials are increasing with time in the same direction as the compressive radial stress histories. That is the electric potential histories are induced by the compressive radial stress histories during creep deformation of the FGPM cylinder.

Keywords: Time-dependent; Thermo-electro-mechanical creep; Stress histories; Electric potential histories; FGPM Rotating cylinder.

1 INTRODUCTION

PIEZOEFFECT has important uses in modern engineering because it expresses the connection between the electrical and mechanical fields which has wide applications in electro-mechanical devices, such as actuators, sensors and transducers. Recently, a new class of composite materials known as functionally graded materials (FGMs) has drawn considerable attention. A typical FGM, with a high bending–stretching coupling effect, is an inhomogeneous composite made from different phases of material constituents (usually ceramic and metal) which used in, nuclear, aircraft, space engineering and pressure vessels.

Thermoelectroelastic analysis of FGPM components has been investigated by many researchers. Mechanical and thermal stresses in a functionally graded hollow cylinder due to radially symmetric were investigated by Jabbari et al. [1]. Analysis of the thermal stress behavior of functionally graded hollow circular cylinders was presented by Liew et al. [2]. You [3] presented elastic analysis of internally pressurized thick-walled spherical pressure vessels of functionally graded materials. Dai et al. [4] studied exact solutions for functionally graded pressure vessels in a uniform magnetic field. Coupled thermoelasticity of functionally graded cylindrical shells was developed by Bahtui

* Corresponding author. Tel.: +98 913 162 6594; Fax: +98 361 591 2424.
E-mail address: aghorban@kashanu.ac.ir (A. Ghorbanpour Arani).

and Eslami [5]. Recently, Ghorbanpour Arani et al. [6] investigated the effect of material in-homogeneity on electro-thermo-mechanical behaviors of functionally graded piezoelectric rotating shaft. Also, they [7] studied electro-thermo-mechanical behaviors of FGPM spheres using analytical method and ANSYS software.

None of the above solutions have considered creep deformation of the FGPM cylinders. Pai [8] investigated steady-state creep analysis of thick-walled orthotropic cylinders. Sim and Penny [9] analyzed plane strain creep behavior of thick-walled cylinders. Bhatnagar and Arya [10] investigated large strain creep deformation of a thick-walled cylinder of an anisotropic material subjected to internal pressure. Simonian [11] calculated the thermal stresses in thick-walled cylinders taking account of non-linear creep. Yang [12] presented a solution for time-dependent creep behavior of FGM cylinders using Norton's law for material creep constitutive model. Steady-state creep of a pressurized thick cylinder in both the linear and the power law ranges was investigated by Altenbach et al. [13]. Loghman et al. [14] studied the magnetothermoelastic creep analysis of functionally graded cylinders. They found that radial stress redistributions are not significant for different material properties, however, major redistributions occur for circumferential and effective stresses. Recently, semi-analytical solution of time-dependent electro-thermo-mechanical creep for radially polarized piezoelectric cylinder was investigated by Ghorbanpour Arani et al. [15]. It has been shown by Zhou and Kamlah [16] that even at room temperature ferroelectric piezoceramics exhibit significant creep effects. This creep is of a primary type and can be expressed by a power law constitutive model. To improve the performance and reliability of piezoactuators used for high-precision applications, time-dependent creep analysis must be considered when these devices are used even at room temperatures.

Apart from a couple of studies, prepared by a few authors here, little or no reference has been made so far in the literature on the time-dependent creep analysis of piezoelectric cylinders. In this study history of stresses, deformation and electric potential of a thick hollow FGM rotating cylinder made of radially polarized anisotropic piezoelectric material, e.g., PZT-7A is investigated using a semi-analytical method base on Mendelson's method of successive elastic solution.

2 HEAT CONDUCTION PROBLEM

In this study, a distributed temperature field due to steady-state heat conduction has been considered. The steady-state, heat transfer equation in the FGPM cylinder with inner radius a and outer radius b is solved with the assumed boundary conditions [7]:

$$\frac{1}{r}\left(rK(r)T'(r)\right)' = 0 \tag{1}$$

$$A_{11}T'(a) + A_{12}T(a) = f_1$$
$$A_{21}T'(b) + A_{22}T(b) = f_2 \tag{2}$$

where (′) denotes differentiation with respect to r, $K=K(r)$ is the thermal conductivity, A_{ij} (i,j=1,2) and either designate the thermal conductivity or the heat transfer coefficient and the constants f_1 and f_2 have known values on the inner and outer radius, respectively. It is assumed that the non-homogeneous thermal conductivity $K(r)$ is a power function of the radius

$$K(r) = K_0 r^{\gamma} \tag{3}$$

where γ is in-homogeneity material parameter. Using Eq. (3) into Eq. (1) for the thermal conductivity, the heat conduction equation can be written as

$$\frac{1}{r}(K_0 r^{\gamma+1}T'(r))' = 0 \tag{4}$$

Integrating Eq. (4) yields

$$T(r) = -\frac{A_1}{\gamma} r^{-\gamma} + A_2 \tag{5}$$

Applying the boundary conditions (2) results in the following relations for the coefficients A_1 and A_2

$$A_1 = \frac{A_{22} f_1 - A_{12} f_2}{A_{22}\left(A_{11} r_a^{-(1+\gamma)} - A_{12}\dfrac{r_a^{-\gamma}}{\gamma}\right) - A_{12}\left(A_{21} r_b^{-(1+\gamma)} - A_{22}\dfrac{r_b^{-\gamma}}{\gamma}\right)} \tag{6}$$

$$A_2 = \frac{f_2\left(A_{11} r_a^{-(1+\gamma)} - A_{12}\dfrac{r_a^{-\gamma}}{\gamma}\right) - f_1\left(A_{21} r_b^{-(1+\gamma)} - A_{22}\dfrac{r_b^{-\gamma}}{\gamma}\right)}{A_{22}\left(A_{11} r_a^{-(1+\gamma)} - A_{12}\dfrac{r_a^{-\gamma}}{\gamma}\right) - A_{12}\left(A_{21} r_b^{-(1+\gamma)} - A_{22}\dfrac{r_b^{-\gamma}}{\gamma}\right)}. \tag{7}$$

Dimensionless temperature distribution obtained from Eq. (5) for different values of in-homogeneity material parameter γ is shown in Fig. 1.

3 BASIC FORMULATION OF ROTATING HOLLOW FGPM CYLINDER

A hollow FGPM cylinder rotating about its axis at constant angular velocity ω, with inner and outer radius of *a* and *b* subjected to an inner pressure, thermal gradient and an electric potential is considered Fig. 2. The components of displacement and electric potential are assumed:

$$U_r = u(r), \qquad U_z = 0, \qquad U_\theta = 0, \qquad \phi = \phi(r) \tag{8}$$

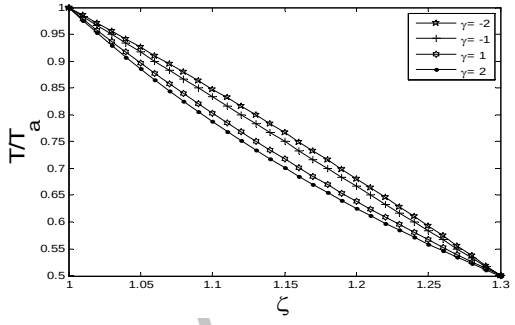

Fig. 1
Temperature distribution of the FGPM cylinder for different values of γ.

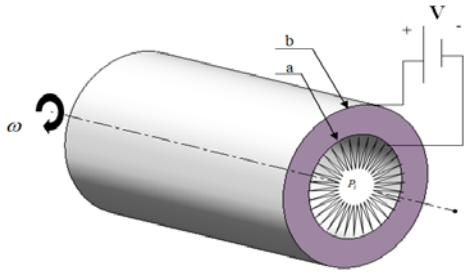

Fig. 2
Hollow FGPM rotating circular shaft subject to uniform temperature field, uniform internal pressure, uniform external pressure and applied voltage V.

The equation of equilibrium considering the inertia body force and the Maxwell's equation for free electric charge density are written as [15]:

$$\frac{\partial \sigma_{rr}}{\partial r}+\frac{\sigma_{rr}-\sigma_{\theta\theta}}{r}+\rho_0 r\omega^2=0 \tag{9}$$

$$\frac{\partial D_{rr}}{\partial r}+\frac{D_{rr}}{r}=0 \tag{10}$$

where $\sigma_{ii}\ (i=r,\theta)$ and D_{rr} are the stress tensor and electric displacement, respectively. Also, the strain-displacement and the relation between electric field and electric potential are reduced as [15]

$$\varepsilon_{rr}=\frac{\partial u}{\partial r} \tag{11}$$

$$\varepsilon_{\theta\theta}=\frac{u}{r} \tag{12}$$

$$E_{rr}=-\frac{\partial \phi}{\partial r} \tag{13}$$

The constitutive relations of cylindrically orthotropic radially polarized piezoelectric media and the component of radial electric displacement vector also can be written as [17-19]:

$$\sigma_{rr}=c_{11}\varepsilon_{rr}+c_{12}\varepsilon_{\theta\theta}-c_{11}\varepsilon^{c}_{rr}-c_{12}\varepsilon^{c}_{\theta\theta}-(c_{11}\alpha_r+c_{12}\alpha_\theta)T(r)-e_{11}E_{rr} \tag{14}$$

$$\sigma_{\theta\theta}=c_{12}\varepsilon_{rr}+c_{22}\varepsilon_{\theta\theta}-c_{12}\varepsilon^{c}_{rr}-c_{22}\varepsilon^{c}_{\theta\theta}-(c_{12}\alpha_r+c_{22}\alpha_\theta)T(r)-e_{12}E_{rr} \tag{15}$$

$$D_{rr}=e_{11}\varepsilon_{rr}+e_{12}\varepsilon_{\theta\theta}-e_{11}\varepsilon^{c}_{rr}-e_{12}\varepsilon^{c}_{\theta\theta}-(e_{11}\alpha_r+e_{12}\alpha_\theta)T(r)+\in_{11} E_{rr} \tag{16}$$

where $c_{ij}\ (i,j=1,2)$, $e_{1i}\ (i=1,2)$, $\alpha_i\ (i=r,\theta)$ and $\in_{11}$ are elastic constants, piezoelectric constants, thermal expansion coefficients, dielectric constants, respectively.

For the analysis, the following dimensionless quantities are introduced as:

$$\sigma_i=\frac{\sigma_{ii}}{c_{22}}\ (i=r,\theta),\qquad c_i=\frac{c_{1i}}{c_{22}}\ (i=1,2),\qquad E_i=\frac{e_{1i}}{\sqrt{C_{22}\in_{11}}}\ (i=1,2),\qquad D_r=\frac{D_{rr}}{\sqrt{C_{22}\in_{11}}},$$
$$u=\frac{u_r}{a},\qquad \xi=\frac{r}{a},\qquad \eta=\frac{b}{a},\quad \beta=\frac{\beta_1}{\sqrt{C_{22}\in_{11}}},\qquad \Omega=\frac{a^2\rho_0\omega^2}{c_{22}},\qquad \Phi=\frac{\varphi}{a\sqrt{\frac{c_{22}}{\in_{11}}}} \tag{17}$$

Using the above dimensionless variables, Eqs. (5), (9) and (10) can be expressed as:

$$T(\xi)=-\frac{A_1}{\gamma}\xi^{-\gamma}+A_2 \tag{18}$$

$$\frac{\partial \sigma_r}{\partial \xi}+\frac{\sigma_r-\sigma_\theta}{\xi}+\Omega\xi=0 \tag{19}$$

$$\frac{\partial D_r}{\partial \xi}+\frac{D_r}{\xi}=0 \tag{20}$$

Before substituting the component of the electric field in Maxwell's equation, appropriate functions for all properties are assumed as [7]:

$$\Psi_r = \Psi_0 \left(\frac{r}{a}\right)^{\gamma} \tag{21}$$

in which Ψ_r represents the general properties of the cylinder such as the elastic, piezoelectric, and dielectric coefficients, and Ψ_0 corresponds to the value of the coefficients at the outer surface. Substituting Eqs. (17) and (21) into Eqs. (14-16) the two components of the stresses and the radial electric displacement are obtained as:

$$\sigma_r = \xi^{\gamma}\left(c_1\frac{\partial u}{\partial \xi} + c_2\frac{u}{\xi} - c_1\varepsilon_{rr}^c - c_2\varepsilon_{\theta\theta}^c - \xi^{\gamma}(c_1\alpha_r + c_2\alpha_\theta)T(\xi) + E_1\frac{\partial \Phi}{\partial \xi}\right) \tag{22}$$

$$\sigma_\theta = \xi^{\gamma}\left(c_2\frac{\partial u}{\partial \xi} + \frac{u}{\xi} - c_2\varepsilon_{rr}^c - \varepsilon_{\theta\theta}^c - \xi^{\gamma}(c_2\alpha_r + \alpha_\theta)T(\xi) + E_2\frac{\partial \Phi}{\partial \xi}\right) \tag{23}$$

$$D_r = \xi^{\gamma}\left(E_1\frac{\partial u}{\partial \xi} + E_2\frac{u}{\xi} - E_1\varepsilon_{rr}^c - E_2\varepsilon_{\theta\theta}^c - \xi^{\gamma}(E_1\alpha_r + E_2\alpha_\theta)T(\xi) - \frac{\partial \Phi}{\partial \xi}\right) \tag{24}$$

4 SOLUTION PROCEDURE

The solution of Eq. (20) is

$$D_r = \frac{F_1}{\xi} \tag{25}$$

where F_1 is a integration constant. Substituting Eq. (25) into Eq. (16), we obtain

$$\frac{\partial \Phi}{\partial \xi} = -\frac{F_1}{\xi}\xi^{-\gamma} + E_1\frac{\partial u}{\partial \xi} + E_2\frac{u}{\xi} - E_1\varepsilon_{rr}^c - E_2\varepsilon_{\theta\theta}^c - \xi^{\gamma}(E_1\alpha_r + E_2\alpha_\theta)T(\xi) \tag{26}$$

Substituting Eq. (26) into Eqs. (14) and (15), leads to

$$\sigma_r = \xi^{\gamma}\left(J_1\left(\frac{\partial u}{\partial \xi} - \varepsilon_{rr}^c - \xi^{\gamma}\alpha_r T(\xi)\right) + J_2\left(\frac{u}{\xi} - \varepsilon_{\theta\theta}^c - \xi^{\gamma}\alpha_\theta T(\xi)\right) - \frac{E_1F_1}{\xi}\xi^{-\gamma}\right) \tag{27}$$

$$\sigma_\theta = \xi^{\gamma}\left(J_2\left(\frac{\partial u}{\partial \xi} - \varepsilon_{rr}^c - \xi^{\gamma}\alpha_r T(\xi)\right) + J_3\left(\frac{u}{\xi} - \varepsilon_{\theta\theta}^c - \xi^{\gamma}\alpha_\theta T(\xi)\right) - \frac{E_2F_1}{\xi}\xi^{-\gamma}\right) \tag{28}$$

where

$$J_1 = C_1 + E_1^2, \qquad J_2 = C_2 + E_1E_2, \qquad J_3 = 1 + E_2^2 \tag{29}$$

Electric potential Φ is obtained by integrating the Eq. (26)

$$\Phi = \int\left(E_1\frac{\partial u}{\partial \xi} + E_2\frac{u}{\xi} - E_1\varepsilon_{rr}^c - E_2\varepsilon_{\theta\theta}^c - \xi^{\gamma}(E_1\alpha_r + E_2\alpha_\theta)T(\xi) - \frac{F_1}{\xi}\xi^{-\gamma}\right)\mathrm{d}\xi \tag{30}$$

Finally, substituting Eqs. (27) and (28) into Eq. (19) yields the following in-homogeneous ordinary differential equation containing time-dependent creep strains

$$\xi^2\frac{\partial^2 u}{\partial\xi^2}+\xi J_4\frac{\partial u}{\partial\xi}+J_5 u=-A_1J_6\xi-A_2J_7\xi^{1+\gamma}-F_1J_8\xi^{-\gamma}-J_9\xi^3-J_{10}\,\xi\varepsilon_{rr}^c-J_{11}\,\xi\varepsilon_{\theta\theta}^c+\xi^2\frac{\partial\varepsilon_{rr}^c}{\partial\xi}+J_{12}\xi^2\frac{\partial\varepsilon_{\theta\theta}^c}{\partial\xi} \tag{31}$$

where

$$\begin{aligned}
&J_4=\frac{J_1(1+\gamma)}{J_1},\qquad J_5=\frac{\gamma J_2-J_3}{J_1},\qquad J_6=\frac{(\gamma J_1+J_1-J_2)\alpha_r+(\gamma J_2+J_2-J_3)\alpha_\theta}{J_1}\\
&J_7=\frac{(-2\gamma J_1-J_1+J_2)\alpha_r+(-2\gamma J_2-J_2+J_3)\alpha_\theta}{J_1},\qquad J_8=\frac{E_2}{J_1},\qquad J_9=\frac{\Omega}{J_1}\\
&J_{10}=\frac{-\gamma J_1-J_1+J_2}{J_1},\qquad J_{11}=\frac{-\gamma J_2-J_2+J_3}{J_1},\qquad J_{12}=\frac{-J_2}{J_1},\qquad J_{13}=\frac{D_5(1+\gamma)-D_7}{D_1}
\end{aligned} \tag{32}$$

Eq. (31) is a non-homogeneous second-order ordinary differential equation containing time-dependent creep strains for displacement field in the FGPM hollow rotating cylinder.

4.1 Semi-analytical solution for thermo-electro- elastic analysis of rotating cylinder

A semi-analytical method for solution of the differential Eq. (31) has been applied. The solution domain is first divided into some finite divisions. The coefficients of Eq. (31) are evaluated at ξ^m, mean radius of m^{th} division, and therefore, the differential equation with constant coefficients become valid only for the m^{th} sub-domain which can be re-written as [20, 21]:

$$\left(P_1^m\frac{d^2}{dr^2}+P_2^m\frac{d}{dr}+P_3^m\right)u^m+P_4^m=0 \tag{33}$$

$$P_1^m=(\xi^m)^2 \tag{34}$$

$$P_2^m=J_4\xi^m \tag{35}$$

$$P_3^m=J_5 \tag{36}$$

$$\begin{aligned}
P_4^m=&J_6A_1\xi^m+J_7A_2(\xi^m)^{(1+\gamma)}+J_8F_1(\xi^m)^{(-\gamma)}+J_9(\xi^m)^3\\
&+(J_{10}\,\varepsilon_r^c\big|_{\xi=\xi^m}+J_{11}\,\varepsilon_\theta^c\big|_{\xi=\xi^m})\xi^m+\left(-\frac{\partial\varepsilon_r^c}{\partial\xi}\bigg|_{\xi=\xi^m}+J_{12}\,\frac{\partial\varepsilon_\theta^c}{\partial\xi}\bigg|_{\xi=\xi^m}\right)(\xi^m)^2
\end{aligned} \tag{37}$$

Hence, the differential equation can now be solved since the terms corresponding to the creep strain functions on the R.H.S have become known. The general solution for Eq. (33) could be written as follows:

$$u_g^m=\underbrace{K_1{}^m e^{q_1{}^m\xi}}_{u_{g1}^m}+\underbrace{K_2{}^m e^{q_2{}^m\xi}}_{u_{g2}^m} \tag{38}$$

where

$$q_1{}^m,q_2{}^m=\frac{-P_2{}^m\pm\sqrt{(P_2{}^m)^2-4P_3{}^mP_1{}^m}}{2P_1^m} \tag{39}$$

The particular solution of the differential Eq. (33) may be obtained according to the Lagrangian method as:

$$u_p^m = \xi^{q_1^m} u_1^m + \xi^{q_2^m} u_2^m \tag{40}$$

where

$$u_1^m = -\int \frac{\xi^{q_2^m} R(\xi)\big|_{\xi=\xi^m}}{W(q_1^m, q_2^m)\big|_{\xi=\xi^m}}, \qquad u_2^m = \int \frac{\xi^{q_1^m} R(\xi)\big|_{\xi=\xi^m}}{W(q_1^m, q_2^m)\big|_{\xi=\xi^m}} \tag{41}$$

is defined as $W(\xi)$ is the expression on the R.H.S. of Eq. (33) and $R(\xi)$ in which

$$W(q_1^m, q_2^m) = \begin{vmatrix} u_{g1}^m & u_{g2}^m \\ (u_{g1}^m)' & (u_{g2}^m)' \end{vmatrix} \tag{42}$$

In terms of the non-dimensional radial coordinate is therefore written as:

$$\xi^m - \frac{h^m}{2} \le \xi \le \xi^m + \frac{h^m}{2}, \qquad u^m = u_g^m + u_p^m \tag{43}$$

where h^m is the thickness of m^{th} division. Substituting the displacement from Eq. (43) into Eq. (27), (28) and (30) the radial and circumferential stresses and electric potential are evaluated.

The unknowns K_1^m, K_2^m, A_1^m, A_2^m, F_1^m and F_2^m (the constant of integrating of Eq. (30)) are determined by applying the necessary boundary conditions between two adjacent sub-domains. For this purpose, the continuity of radial displacement, radial stress, temperature and electric potential are imposed at the interfaces of the adjacent sub-domains. These continuity conditions at the interfaces are [15]:

$$\begin{aligned}
&u^m\Big|_{\xi=\xi^m+\frac{h^m}{2}} = u^{m+1}\Big|_{\xi=\xi^{m+1}-\frac{h^{m+1}}{2}} \\
&\frac{\mathrm{d}u^m}{\mathrm{d}\xi}\bigg|_{\xi=\xi^m+\frac{h^m}{2}} = \frac{\mathrm{d}u^{m+1}}{\mathrm{d}\xi}\bigg|_{\xi=\xi^{m+1}-\frac{h^{m+1}}{2}} \\
&\sigma_r^m\Big|_{\xi=\xi^m+\frac{h^m}{2}} = \sigma_r^{m+1}\Big|_{\xi=\xi^{m+1}-\frac{h^{m+1}}{2}} \\
&\Phi^m\Big|_{\xi=\xi^m+\frac{h^m}{2}} = \Phi^{m+1}\Big|_{\xi=\xi^{m+1}-\frac{h^{m+1}}{2}} \\
&T_\xi^m\Big|_{\xi=\xi^m+\frac{h^m}{2}} = T_\xi^m\Big|_{\xi=\xi^{m+1}+\frac{h^{m+1}}{2}} \\
&\frac{\partial T_\xi^m}{\partial \xi}\bigg|_{\xi=\xi^m+\frac{h^m}{2}} = \frac{\partial T_\xi^m}{\partial \xi}\bigg|_{\xi=\xi^{m+1}+\frac{h^{m+1}}{2}}
\end{aligned} \tag{44}$$

and global boundary conditions are written in dimensionless form as:

$$\text{(with electric potential)} \quad \Phi(\eta)=0, \quad \Phi(1)=1, \quad \sigma_r(\eta)=0, \quad \sigma_r(1)=-1 \tag{45a}$$

$$\text{(without electric potential)} \quad \Phi(\eta)=0, \quad \Phi(1)=0, \quad \sigma_r(\eta)=0, \quad \sigma_r(1)=-1 \tag{45b}$$

The continuity conditions Eq. (44) together with the global boundary conditions Eqs. (45) yield a set of linear algebraic equations in terms of K_1^m, K_2^m, A_1^m, A_2^m, B_1^m and B_2^m. Solving the resultant linear algebraic equations

the unknown coefficients are calculated. Then the displacement component, the stresses and the electric potential are determined in each radial sub-domain. Increasing the number of divisions improves the accuracy of the results.

4.2 Time-dependent thermo-electro- elastic creep behavior of cylinder

To obtain time-dependent stresses and electric potential, the creep strains in Eqs. (27), (28) and (30) must be considered. Creep strain rates are related to the material creep constitutive model and the current stress tensor by the well known Prandtl–Reuss relation. In this case, Prandtl-Reuss relation is written as [19]:

$$\dot{\varepsilon}_r = \frac{\dot{\varepsilon}_e}{\sigma_e}\left[\sigma_r - 0.5(\sigma_\theta + \sigma_z)\right] \tag{46}$$

$$\dot{\varepsilon}_\theta = \frac{\dot{\varepsilon}_e}{\sigma_e}\left[\sigma_\theta - 0.5(\sigma_r + \sigma_z)\right] \tag{47}$$

$$\dot{\varepsilon}_z = \frac{\dot{\varepsilon}_e}{\sigma_e}\left[\sigma_z - 0.5(\sigma_\theta + \sigma_r)\right] \tag{48}$$

For plane strain condition the axial strain rate disappears, i.e. $\dot{\varepsilon}_z = 0$.

$$\sigma_z = 0.5(\sigma_\theta + \sigma_r) \tag{49}$$

Substituting Eq. (49) into the first two of Eqs. (47) and (48), radial and circumferential strain rates are found to be:

$$\dot{\varepsilon}_r = \frac{3\dot{\varepsilon}_e}{4\sigma_e}(\sigma_r - \sigma_\theta) \tag{50}$$

$$\dot{\varepsilon}_\theta = \frac{3\dot{\varepsilon}_e}{4\sigma_e}(\sigma_\theta - \sigma_r) \tag{51}$$

The Norton's creep constitutive model for FGPM is considered to be [22, 23]:

$$\dot{\varepsilon}_e = B(r)\sigma_e^{n(r)} \tag{52}$$

where

$$n(\xi) = n_0, \qquad B(\xi) = B_0\xi^{-b_1} \tag{53}$$

In this case, the Von Mises equivalent stress is reduced to:

$$\sigma_e = \frac{1}{\sqrt{2}}\sqrt{(\sigma_\theta - \sigma_r)^2 + (\sigma_\theta - \sigma_z)^2 + (\sigma_z - \sigma_r)^2} = \frac{\sqrt{3}}{2}(\sigma_\theta - \sigma_r) \tag{54}$$

To obtain history of stresses, deformation and electric potential a numerical procedure based on the method of successive approximation has been tailored.

5 NUMERICAL PROCEDURE

We have employed Mendelson's method of successive elastic solution to obtain history of stresses, displacement and electric potential as follows:

1- An appropriate time step is selected. In this solution, the first time increment is selected as $\Delta t = 6$ month. The total time is the sum of time increments as the creep process progresses in time. For the ith timing stop, the total time is $t_i = \sum_{k=1}^{i-1} \Delta t_k + \Delta t_i$.

2- Thickness of the FGPM cylinder is divided into N equal divisions. Initial values of $\Delta\varepsilon^c_{r,ij} = -0.00001, \Delta\varepsilon^c_{\theta,ij} = 0.00001$ for radial and circumferential creep strain increments are estimated at all division points throughout thickness. These are added to the accumulated creep strains obtained from the previous timing step at all division points throughout the FGPM cylinder as

$$\varepsilon^c_{r,ij} = \sum_{k=1}^{i-1} \Delta\varepsilon^c_{r,kj} + \Delta\varepsilon^c_{r,ij}, \qquad \varepsilon^c_{\theta,ij} = \sum_{k=1}^{i-1} \Delta\varepsilon^c_{\theta,kj} + \Delta\varepsilon^c_{\theta,ij}$$

where the subscripts *i* and *j* indicate the timing step and division point respectively.

3- These accumulated creep strains are substituted in Eqs. (27), (28) and (30). This differential equation can be solved for the displacement at m^{th} layer. Using local and global boundary conditions the displacements, stresses and electric potentials at time t_i are determined.

4- Effective stresses are then calculated at all division points. $\sigma_{e,ij} = \frac{\sqrt{3}}{2}\left|\sigma_{\theta,ij} - \sigma_{r,ij}\right|$.

5- Effective creep strain rates are then calculated at all division points (j) for i*th* timing step using Norton's creep constitutive model as $\dot{\varepsilon}_{e,ij} = B(\xi_j)\sigma_{e,ij}^{n_0}$.

6- From Prandtl-Reuss relation radial and circumferential creep strain rates are obtained as follows:

$$\dot{\varepsilon}_{r,ij} = \frac{3\dot{\varepsilon}_{e,ij}}{4\sigma_{e,ij}}(\sigma_{r,ij} - \sigma_{\theta,ij}), \qquad \dot{\varepsilon}_{\theta,ij} = \frac{3\dot{\varepsilon}_{e,ij}}{4\sigma_{e,ij}}(\sigma_{\theta,ij} - \sigma_{r,ij}).$$

7- New values for radial and circumferential creep strain increments at all division points are then calculated using the above creep strain rates and the time increment as follows:

$$\Delta\varepsilon^{c,new}_{r,ij} = \dot{\varepsilon}^c_{r,ij} \times \Delta t_i, \qquad \Delta\varepsilon^{c,new}_{\theta,ij} = \dot{\varepsilon}^c_{\theta,ij} \times \Delta t_i.$$

These new obtained values for creep strain increments are compared with the initial estimated values at all division points for the convergence of the procedure. If convergence is obtained, time is advanced one increment and the procedure is repeated for the new time increment from step 1. If convergence is not satisfied, these new obtained values of creep strain increments will be considered as initial values and the procedure will be repeated from step 2 until convergence is obtained. From the above numerical procedure history of stresses, deformations and electric potential are obtained for FGPM cylinder and illustrated in Figs. 3 to 22

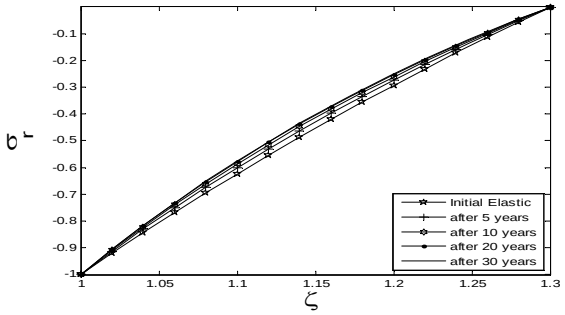

Fig. 3
History of radial stress for the FGPM cylinder for the case $\gamma = 2$.

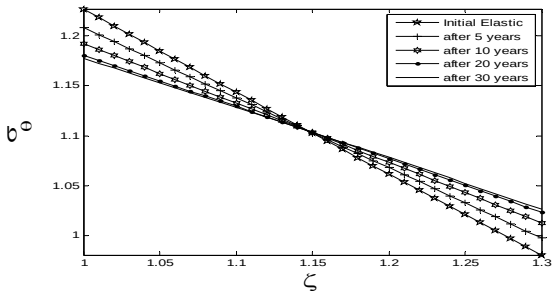

Fig. 4
History of circumferential stress for the FGPM cylinder for the case $\gamma = 2$.

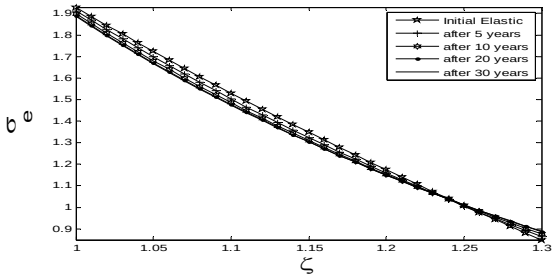

Fig. 5
History of effective stress for the FGPM cylinder for the case $\gamma = 2$.

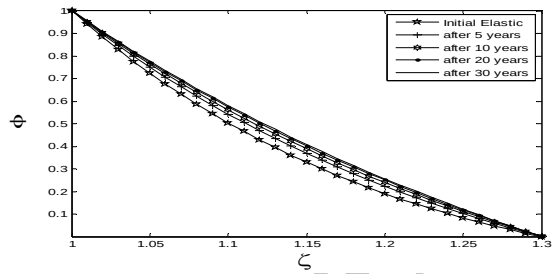

Fig. 6
History of electric potential for the FGPM cylinder for the case $\gamma = 2$.

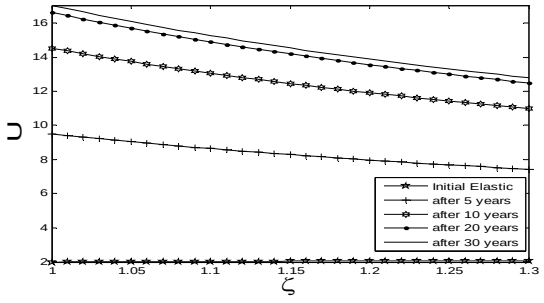

Fig. 7
History of displacement for the FGPM cylinder for the case $\gamma = 2$.

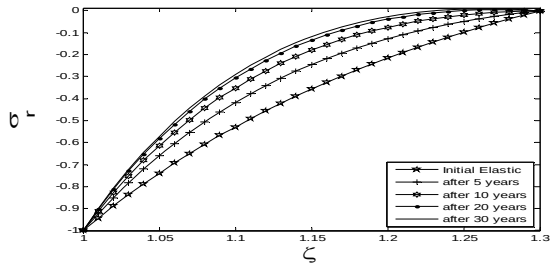

Fig. 8
History of radial stress for the FGPM cylinder for the case $\gamma = -2$.

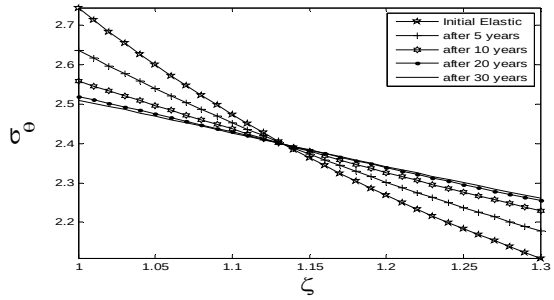

Fig. 9
History of circumferential stress for the FGPM cylinder for the case $\gamma = -2$.

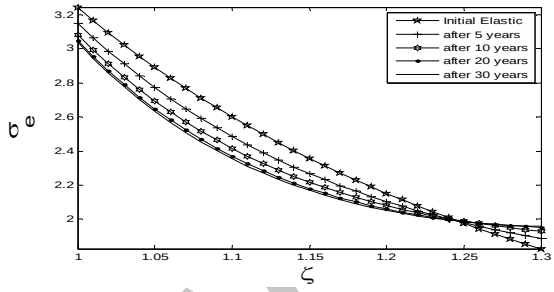

Fig. 10
History of effective stress for the FGPM cylinder for the case $\gamma = -2$.

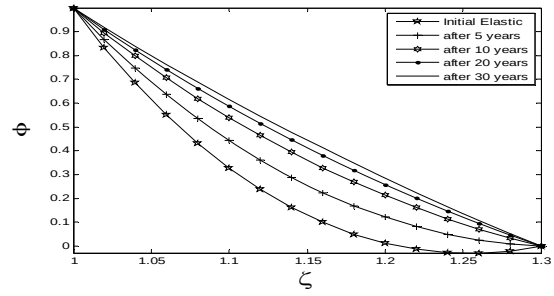

Fig. 11
History of electric potential for the FGPM cylinder for the case $\gamma = -2$.

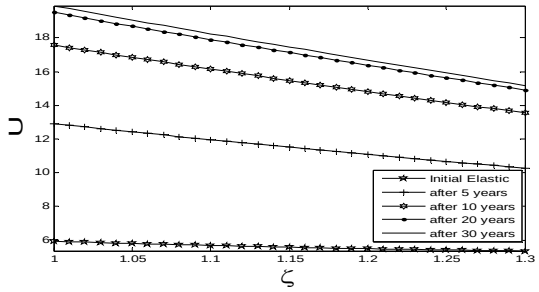

Fig. 12
History of displacement for the FGPM cylinder for the case $\gamma = -2$.

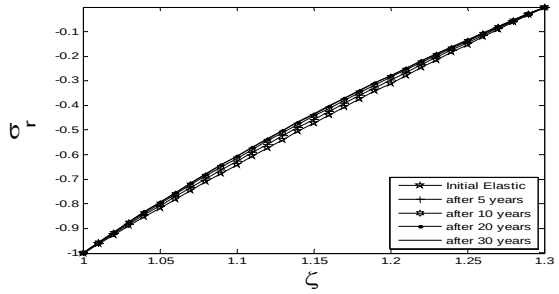

Fig. 13
History of radial stress for the FGPM cylinder for the case $\gamma = 2$.

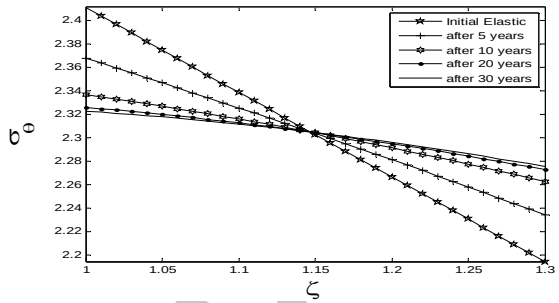

Fig. 14
History of circumferential stress for the FGPM cylinder for the case $\gamma = 2$.

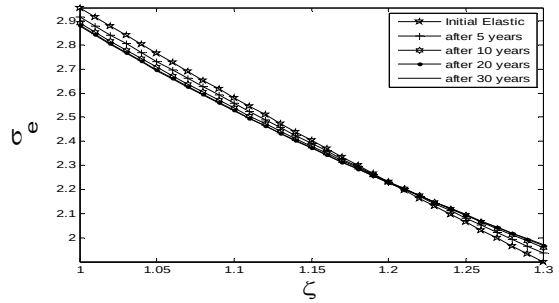

Fig. 15
History of effective stress for the FGPM cylinder for the case $\gamma = 2$.

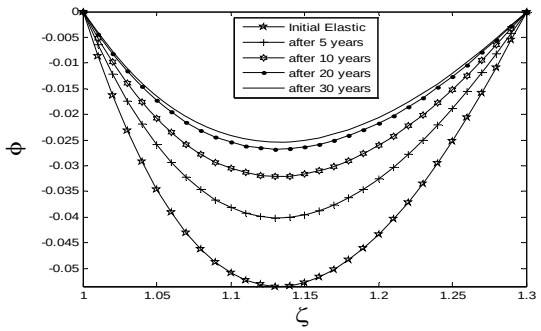

Fig. 16
History of electric potential for the FGPM cylinder for the case $\gamma = 2$.

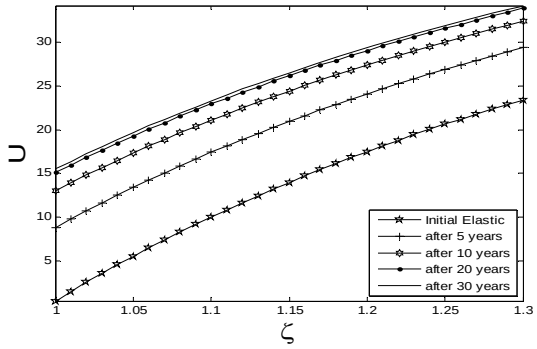

Fig. 17
History of displacement for the FGPM cylinder for the case $\gamma = 2$.

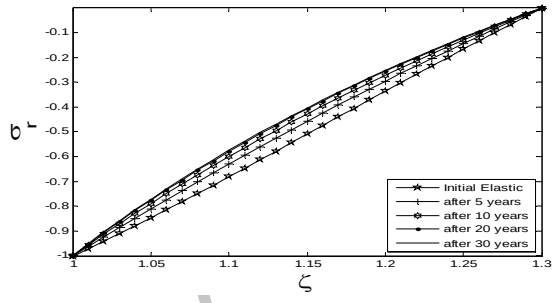

Fig. 18
History of radial stress for the FGPM cylinder for the case $\gamma = -2$.

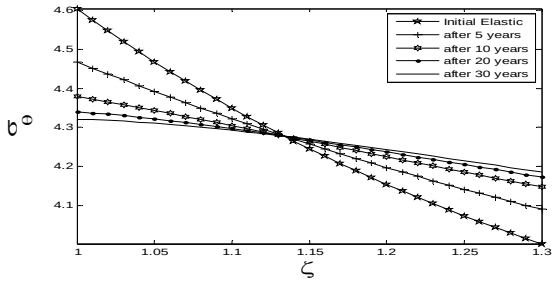

Fig. 19
History of circumferential stress for the FGPM cylinder for the case $\gamma = -2$.

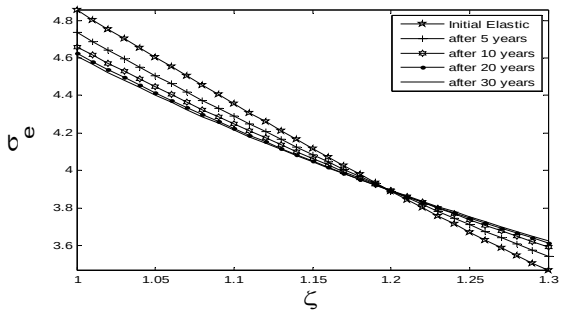

Fig. 20
History of effective stress for the FGPM cylinder for the case $\gamma = -2$.

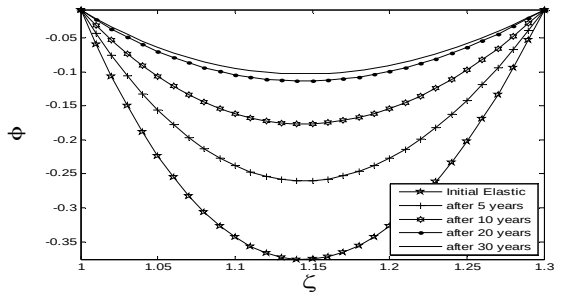

Fig. 21
History of electric potential for the FGPM cylinder for the case $\gamma = -2$.

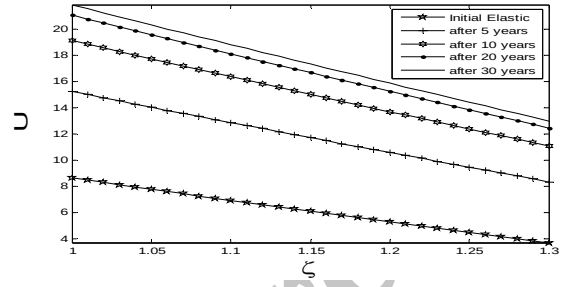

Fig. 22
History of displacement for the FGPM cylinder for the case $\gamma = -2$.

Table 1
Mechanical, electrical and thermal properties for PZT_7A [24]

Property	*PZT_7A*
c_{11}	131 GPa
c_{12}	81.3 GPa
c_{22}	148 GPa
e_{11}	9.50 C/m^2
e_{12}	-2.10 C/m^2
e_{11}	9.4×10^{-9} C^2/Nm^2
α_{r0}	1×10^{-6} 1/K
α_{r0}	2×10^{-6} 1/K
ρ	7600 kg/m^3

6 NUMERICAL RESULTS AND DISCUSSION

The numerical results presented here are based on the material properties defined in Table 1 for PZT-7A. [24] .The temperature at the inner and outer surfaces of the FGPM cylinder are considered to be $T_a = 50^0\text{C}$ and $T_b = 25^0\text{C}$, respectively and the aspect ratio is $\eta = 1.3$.

History of stresses, electric potential and displacement of the FGPM rotating hollow cylinder for two cases of mechanical and electrical boundary conditions Eqs. ((45a) and (45b)) is investigated for different values of material in-homogeneity γ. The results are reported for $\gamma = 2$ and $\gamma = -2$ in this paper. Radial, circumferential and effective stress histories with boundary conditions of Eq. (45a) are illustrated in Figs. 3, 4 and 5 for the case $\gamma = 2$ and in Figs. 8, 9 and 10 for the case $\gamma = -2$. Radial, circumferential and effective stress histories with boundary conditions of Eq. (45b) are illustrated in Figs. 13, 14 and 15 for the case $\gamma = 2$ and in Figs. 18, 19 and 20 for the case $\gamma = -2$. In both cases, radial stresses are constant with time at the inner and outer surfaces of the cylinder satisfying the constant mechanical boundary conditions. However, through-thickness radial stresses are increasing with time at a decreasing rate so that there is a saturation condition beyond which not much change occurs. Indeed after 30 years the solution approaches the steady state condition. Circumferential and effective stresses are decreasing at the inner surface of the FGPM cylinder and increasing at the outer surface with decreasing rates so that they also approach steady state condition after 30 years. Reference stresses are also identified for circumferential and effective stresses which are independent of time. Comparing stresses with and without the effect of electric potential one can find that imposing an electric potential significantly decreases the highly tensile circumferential stresses of the FGPM cylinder. Histories of the imposed electric potentials for the boundary conditions of Eqs. (45a) and (45b) are shown in Figs. 6, 11 and Figs. 16, 21 respectively for two cases of $\gamma = 2$ and $\gamma = -2$. In both cases, the electric potential redistributions satisfy the boundary conditions of the imposed electric potentials at the inner and outer surfaces. However, through-thickness electric potentials are varying with time in the same direction as the compressive radial stress histories. That is the electric potential histories are induced by the compressive radial stress histories during creep deformation of the FGPM cylinder. Comparing stress and electric potential redistributions for $\gamma = 2$ and $\gamma = -2$ one can find that the time rate of change of stresses and electric potentials for $\gamma = -2$ is higher than $\gamma = 2$. History of radial displacements for the boundary conditions of Eqs. (45a) and (45b) are shown in Figs. 7, 12 and Figs. 17, 22 respectively for two cases of $\gamma = 2$ and $\gamma = -2$. It is clear that radial displacements are also increasing with time at a decreasing rate during creep process of the FGPM cylinder and finally approach the steady state condition.

6 CONCLUSIONS

Time-dependent creep analysis has been carried out to improve the performance and reliability of piezoactuators used for high-precision applications, when these devices are used even at room temperatures. Time-dependent thermo-electro-mechanical creep behavior of radially polarized FGPM hollow rotating cylinder is investigated using a semi-analytical numerical method. History of stresses, electric potentials and displacements of two different combinations of mechanical and electrical boundary conditions for two cases of the material in-homogeneity parameter g are studied. The results show that the material in-homogeneity parameter g has a significant effect on the thermo-electro- mechanical creep stresses, electric potential and radial displacement. It has been found that the stress and electric potential redistributions for $\gamma = -2$ is higher than $\gamma = 2$. In general, a major redistribution for electric potential takes place throughout the thickness. Electric potentials are increasing with time in the same direction as the compressive radial stress histories. In fact, the electric potential histories are induced by the compressive radial stress histories during creep deformation of the FGPM cylinder. It has also been concluded that imposing an electric potential significantly decreases the highly tensile tangential stresses.

ACKNOWLEDGEMENTS

The authors would like to thank the referees for their valuable comments. The authors are also grateful to University of Kashan for supporting this work by Grant No. 65475/15.

REFERENCES

[1] Jabbaria M., Sohrabpour S., Eslami M.R., 2002, Mechanical and thermal stresses in a functionally graded hollow cylinder due to radially symmetric loads, *International Journal of Pressure Vessel and Piping* **79**: 493-497.
[2] Liew K.M., Kitipornchai S., Zhang X.Z., Lim C.W., 2003, Analysis of the thermal stress behaviour of functionally graded hollow circular cylinders, *International Journal of Solids and Structures* **40**: 2355-2380.
[3] You L.H., Zhang J.J., You X.Y., 2005, Elastic analysis of internally pressurized thick-walled spherical pressure vessels of functionally graded materials, *International Journal of Pressure Vessel and Piping* **82**: 347-354.
[4] Dai H.L., Fu Y.M., Dong Z.M., 2006, Exact solutions for functionally graded pressure vessels in a uniform magnetic field, *International Journal of Solids and Structures* **43**: 5570-5580.
[5] Bahtui A., Eslami M.R., 2007, Coupled thermoelasticity of functionally graded cylindrical shells, *Mechanics Research Communications* **34**: 1-18.
[6] Ghorbanpour Arani A., Kolahchi R., Mosallaie Barzoki A.A., 2011, Effect of material in-homogeneity on electro-thermo-mechanical behaviors of functionally graded piezoelectric rotating shaft, *Applied Mathematical Modeling* **35**: 2771-2789.
[7] Ghorbanpour Arani A., Kolahchi R., Mosallaie Barzoki A.A., Loghman A., 2011, Electro-thermo-mechanical behaviors of FGPM spheres using analytical method and ANSYS software, *Applied Mathematical* Modeling **36**: 139-157.
[8] Pai D.H., 1967, steady-state creep analysis of thick-walled orthotropic cylinders, *International Journal of Mechanics Science* **9**: 335-482.
[9] Sim R.G., Penny R.K., 1971, Plane strain creep behaviour of thick-walled cylinders, *International Journal of Mechanics Science* **13**: 987-1009.
[10] Bhatnagar N.S., Arya V.K., 1974, Large strain creep analysis of thick-walled cylinders, *International Journal of Non-Linear Mechanics* **9**: 127-40.
[11] Simonian A.M., 1979, Calculation of thermal stresses in thick-walled cylinders taking account of non-linear creep, *International Journal of Engineering Science* **17**: 513-522.
[12] Yang Y.Y., 2000, Time-dependent stress analysis in functionally graded materials, *International Journal of Solids and Structures* **37**: 7593-7608.
[13] Altenbach H., Gorash Y., Naumenko K., 2008, Steady-state creep of a pressurized thick cylinder in both the linear and the power law ranges, *Acta Mechanica* **195**: 263-274.
[14] Loghman A., Ghorbanpour Arani A., Amir S., Vajedi A., 2010, Magneto thermoelastic creep analysis of functionally graded cylinders, *International Journal of Pressure Vessel and Piping* **87**: 389-395.
[15] Ghorbanpour Arani A., Mosallaie Barzoki A.A., Kolahchi R., Mozdianfard M.R., Loghman A., 2011, Semi-analytical solution of time-dependent electro-thermo-mechanical creep for radially polarized piezoelectric cylinder, *Computer and Structures* **89**: 1494-1502.
[16] *Zhou D., Kamlah M., 2006,* Room-temperature creep of soft PZT under static electrical and compressive stress loading, *Acta Materialia* **54**: 1389-1396.
[17] Tiersten H.F., 1969, *Linear piezoelectric plate vibrations*, Plenum Press, New York.
[18] Fungn Y.C., 1965, *Foundations of solid mechanics*, Prentice-Hall, New York.
[19] Mendelson A., 1968, *Plasticity Theory and Applications*, Macmillan, New York.
[20] Kordkheili S.A.H., Naghdabadi R., 2007, Thermoelastic analysis of a functionally graded rotating disk, *Computer and Structures* **79**: 508-516.
[21] Bayat M., Saleem M., Sahari B.B., Hamouda A.M.S., Mahdi E., 2009, Mechanical and thermal stresses in a functionally graded rotating disk with variable thickness due to radially symmetry loads, *International Journal of Pressure Vessel and Piping* **86**: 357-372.
[22] Penny R.K., Marriott D.L., 1995, *Design for Creep*, Chapman and Hall, London.
[23] Norton F.H., 1929, *The Creep of Steel at High Temperatures*, McGraw-Hill, London.
[24] Jaffe H., Berlincourt D.A., 1965, Piezoelectric transducer materials, *Proceedings of IEEE* **53**: 1372-1386.